Simulation of droplet dispersion from coughing with consideration of face mask motion

Ayato Takii[1,4], Tatsuya Miyoshi[2], Masashi Yamakawa[2], Yusei Kobayashi[2],

Shinichi Asao[3], Seiichi Takeuchi[3] and Makoto Tsubokura[1,4]

[1] RIKEN Center for Computational Science, Kobe, Hyogo 650-0047, Japan
[2] Kyoto Institute of Technology, Sakyo-ku Kyoto 606-8585, Japan
[3] College of Industrial Technology, Amagasaki Hyogo 661-0047, Japan
[4] Kobe University, Kobe, Hyogo 657-0013, Japan
Ayato.takii@riken.jp

Abstract. Wearing a face mask is widely acknowledged as a critical defense against the transmission of the novel coronavirus (COVID-19) and influenza. This research focuses on the deformation of face masks during a cough and uses fluid dynamics simulations to more precisely predict the trajectory of virus-laden droplets. By employing motion capture technology, we measured the mask's displacement, which reaches up to 6 mm during a cough. Moreover, this paper delves into how the mask's deformation influences the movement of these droplets. We created a model for a small, spherical droplet and analyzed its dispersion by solving its motion equation, factoring in the cough's flow rate, droplet size distribution, and evaporation, all while considering the mask's deformation. Our findings reveal that mask deformation leads to a 7% reduction in average flow velocity compared to analyses using a non-deforming mask. Additionally, the distance droplets disperse increases over time when mask deformation is considered. As a practical application, we analyzed droplet dispersion in a scenario where a wheelchair is being pushed, utilizing airflow data that accounts for mask deformation. This analysis indicated that pushing a wheelchair at a speed of 0.5 m/s significantly raises the infection risk for individuals behind it.

Keywords: COVID-19, Face Mask, Computational Fluid Dynamics

1 Introduction

In 2019, the emergence of a novel coronavirus infection (COVID-19), caused by the SARS-CoV-2 virus, was confirmed [1]. Subsequently, COVID-19 proliferated globally at an explosive rate. Presently, while the trepidation towards the novel coronavirus has diminished among people, it remains important to strategize against potential unknown infectious diseases and mutations of the coronavirus that may arise in the future. Recommended practices for protecting oneself from viral droplets include maintaining social distancing, wearing masks and ensuring adequate ventilation. Due to the challenges in reproducing studies on virus droplets and the complexity of experiments, an

ICCS Camera Ready Version 2024
To cite this paper please use the final published version:
DOI: 10.1007/978-3-031-63783-4_7

engineering approach is efficacious. Notably, research employing Computational Fluid Dynamics (CFD) for numerical simulations has garnered significant attention. Bale et al. [2] developed a framework for quantifying the risk of airborne infections like COVID-19, demonstrating that infection risk decreases as distance from an infected person increases. Yamakawa et al. [3] used a classroom model with ventilation to show that droplets can remain airborne for extended periods, thereby increasing the risk of infection. Bale et al. [4] analyzed the spread of virus droplets during conversations by changing the direction of the wind. In addition, numerical simulations in environments such as classrooms, trains [5], and escalators [6] have been conducted as simulations in applied situations, demonstrating the usefulness of simulating droplet behavior using CFD. Regarding social distancing, Dbouk et al. [7] points out that 2 m is not a sufficient distance. Moreover, Bourouiba et al. [8] revealed that droplets can be dispersed up to 6 to 7 meters indoors. Furthermore, Blocken et al. [9] showed that the range in which droplets fly changes greatly depending on the surrounding airflow environment. Therefore, social distancing alone is insufficient to prevent infection, and it is recommended to wear a mask to reduce the risk of infection. Focusing on masks, Bagchi et al. [10] clarified the behavior of droplets passing through a mask in experiment. In addition, Bourrianne et al. [11] actually filmed people breathing while wearing a mask and showed that the mask moderates the flow rate of exhaled air. In a study using numerical simulations, Pender et al. [12] suggested that social distancing of at least 4 m is required when sneezing while wearing a mask. Additionally, Dbouk et al. [13] revealed that wearing a mask reduces the distance that droplets are spread. As described, studies using numerical simulations regarding masks have revealed the effectiveness of wearing masks in preventing infection and reducing the spread distance of droplets.These studies, however, have adopted static masks that do not deform during coughing or breathing for simplification. If the mask move, it's possible that area of the gap between a mask and face increases and the speed of air leaking decreases. As a result, the traveling distance of viral droplets may be affected. Though many previous literatures have ignored the effect of mask movement on virus droplets, no research has yet verified this. Therefore, we conduct research taking into account the displacement and deformation of masks during coughing to more precisely evaluate the effectiveness of masks in preventing droplet spread. In this paper, we evaluate the influence of mask displacement and deformation due to coughing on the movement of virus droplets. In order to trace the movement of the mask, the displacements of the mask during coughing are measured in experiment. This allows to predict the behavior of virus droplets under conditions close to actual phenomena. Furthermore, numerical simulations with static mask are performed to analyze the effect of considering mask displacement and deformation. Finally, we perform applied calculations to utilize the dynamic mask calculation results.

2 Numerical Approach

2.1 Governing Equations for Fluid Flow

We first calculated fluid flow by coughing, and then analyzed the movement of virus-laden droplets by using the fluid flow data. The continuity equation and the three-

ICCS Camera Ready Version 2024
To cite this paper please use the final published version:
DOI: 10.1007/978-3-031-63783-4_7

dimensional incompressible Navier-Stokes equation used to compute the airflow are as follows:

$$\frac{\partial u}{\partial x}+\frac{\partial v}{\partial y}+\frac{\partial w}{\partial z}=0\,, \tag{1}$$

$$\frac{\partial \boldsymbol{q}}{\partial t}+\frac{\partial \boldsymbol{E}}{\partial x}+\frac{\partial \boldsymbol{F}}{\partial y}+\frac{\partial \boldsymbol{G}}{\partial z}=\left(\frac{\partial \boldsymbol{E_V}}{\partial x}+\frac{\partial \boldsymbol{F_V}}{\partial y}+\frac{\partial \boldsymbol{G_V}}{\partial z}\right), \tag{2}$$

where

$$\boldsymbol{q}=\begin{bmatrix}u\\v\\w\end{bmatrix},\boldsymbol{E}=\begin{bmatrix}u^2+p\\uv\\uw\end{bmatrix},\boldsymbol{F}=\begin{bmatrix}uv\\v^2+p\\vw\end{bmatrix},\boldsymbol{G}=\begin{bmatrix}uw\\vw\\w^2+p\end{bmatrix}$$

$$\boldsymbol{E_V}=\frac{1}{Re}\begin{bmatrix}\partial u/\partial x\\\partial v/\partial x\\\partial w/\partial x\end{bmatrix},\boldsymbol{F_V}=\frac{1}{Re}\begin{bmatrix}\partial u/\partial y\\\partial v/\partial y\\\partial w/\partial y\end{bmatrix},\boldsymbol{G_V}=\frac{1}{Re}\begin{bmatrix}\partial u/\partial z\\\partial v/\partial z\\\partial w/\partial z\end{bmatrix} \tag{3}$$

u, v, w are the corresponding velocity components in the x, y, z direction, respectively, t is time, p is pressure and $Re(\approx 1.6\times 10^4)$ is the Reynolds number with the representative length that is half width of mouth (= 0.02 m) and the representative velocity (= 12.0 m/s). Additionally, $\boldsymbol{E}, \boldsymbol{F}, \boldsymbol{G}$ are the advection vectors, $\boldsymbol{E_V}, \boldsymbol{F_V}, \boldsymbol{G_V}$ are the corresponding viscous stress vectors. Physical variables are defined at cell centers. The governing equations are discretized using the Moving-Grid Finite-Volume Method with an unstructured grid, which is capable of handling moving geometries. This method ensures conservation laws are satisfied even when the computational grid undergoes deformation, such as when the face mask moves and deforms. The specific details are documented in the literature [14]. To solve for incompressible flow, the fractional step method is employed, utilizing the LU-SGS (Lower-Upper Symmetric-Gauss-Seidel) method [15] for the first step and the SOR (Successive Over Relaxation) method for the second step.

2.2 Equation of Motion for Droplets

For calculation of droplets motion, we employed the Lagrangian tracking method [16], assuming that the diameter of the droplets is sufficiently small to consider the effect of the droplets on the fluid negligible. Therefore, we first calculated the fluid flow from coughing, and then simulated the motion of droplets using the flow velocity. Here, droplets were treated as un-deformable spherical droplets, and forces between droplets were ignored. The equation for the motion of droplets is given by:

$$\rho_d V_d\frac{d\boldsymbol{q}_d}{dt}+\rho_d V_d\boldsymbol{g}+\frac{1}{2}C_D\rho_a S_d|\boldsymbol{q}_a-\boldsymbol{q}_d|(\boldsymbol{q}_a-\boldsymbol{q}_d)=0 \tag{4}$$

where the suffixes d and a indicate values pertaining to the droplet and air, respectively. Here, ρ represents density, V is volume, $\boldsymbol{g}$ is gravitational acceleration, $\boldsymbol{q}$ is velocity, C_D is drag coefficient of the droplet. S_d is the projection area of the droplet. The shape of the droplet is assumed to be spherical.

ICCS Camera Ready Version 2024
To cite this paper please use the final published version:
DOI: 10.1007/978-3-031-63783-4_7

3 Measurement of Face Mask Deformation

3.1 Measuring Instrument

Face mask

We used a disposal face mask for the measurement. The size of the face mask is 170 mm × 95 mm. Fig.1 shows a face mask and infrared markers (5 rows and 5 columns a total 25). The diameter of infrared markers was 1.5 mm. They were glued with glue tape, which has few effects on the deformation of the face mask. Here, we assign names to the markers, ranging from I-1 to V-5. Furthermore, some reference markers were placed on face of test subject. By measuring the relative displacement of the reference marker and the marker on the face mask, the displacement of face by coughing can be neglected.

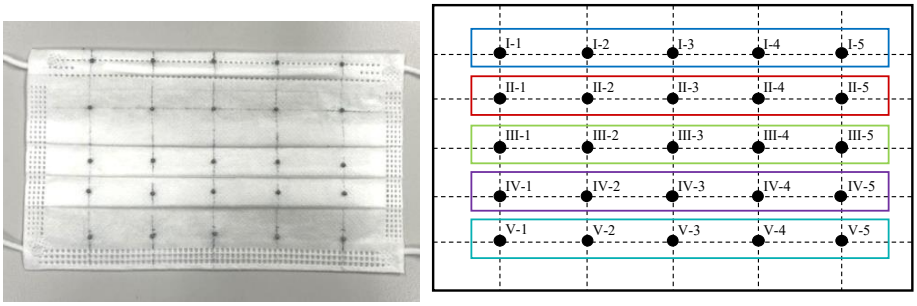

Fig.1. Markers position on the disposal face mask

Motion capture system

To measure the motion of the face mask in three-dimension, we used a motion capture system (OptiTrack motion capture system, Acuity Inc). Fig.2 shows a schematic diagram of the coordinate and configuration of the motion capture system. 6 cameras were placed at a position of about 2 m from the test subject wearing the face mask. To capture all markers from each camera, the cameras were placed at right position. The measurement uncertainty was about 0.015 mm.

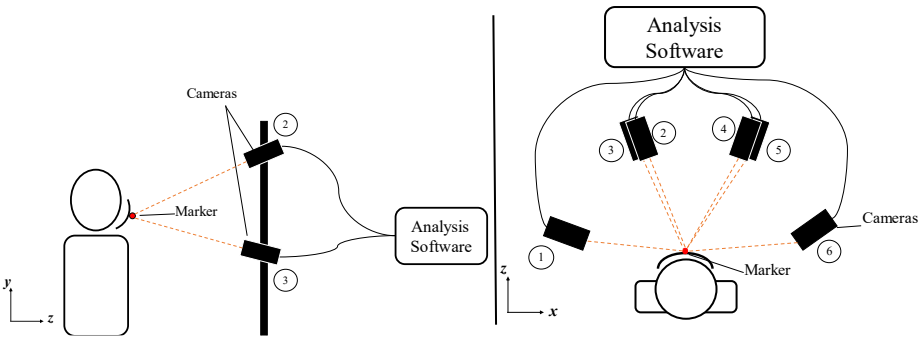

Fig.2. Schematic diagram of motion capture system

ICCS Camera Ready Version 2024
To cite this paper please use the final published version:
DOI: 10.1007/978-3-031-63783-4_7

3.2 Measurement Results

Fig.3 (a) shows the time series of displacement on marker III-2 in first experimental run. It can be seen that the mask reached the maximum displacement of 5.5 mm in the z direction (front of the human body) at ~0.1 seconds after coughing. After coughing ($t \geq 1.0$ s), forward the y and z displacement did not return to the original position because the position of the face mask was displaced by coughing. We considered the deformation in the z direction, since the maximum displacement in x or y direction relating smaller than one in z direction.

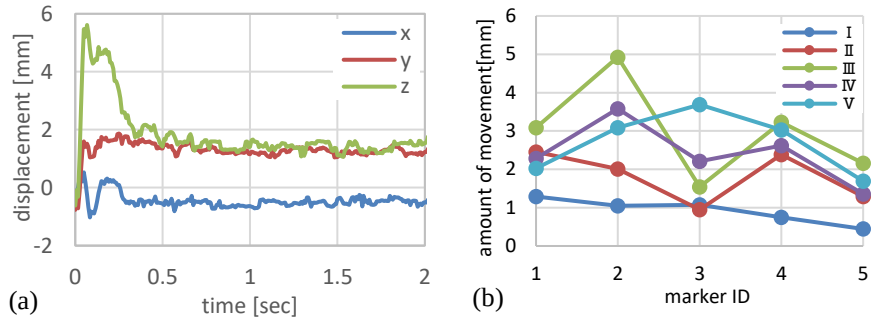

Fig.3. (a) Displacement in each axial direction on marker III-2 and (b) average amount of movement for each marker in forward direction of the face.

Fig.3 (b) displays the ensemble average of the maximum displacement for each marker in the z-direction, based on five experimental runs. We modeled the average displacement by averaging left and right markers to eliminate the asymmetry due to the test subject. The displacement between each marker was calculated by the Lagrange interpolation in x direction and linear interpolation in y direction. The maximum displacement in z direction that was given to the face mask is shown in Fig.4. We modeled the face mask deformation to correlate with the coughing volume flow rate of Gupta et al. [17][18], and the displacement shown in Fig.4 takes the maximum value at $t = 0.1$s after coughing. The displacement tendency in Fig.3 (a) was also modeled by giving a movement to return about 70% to initial position.

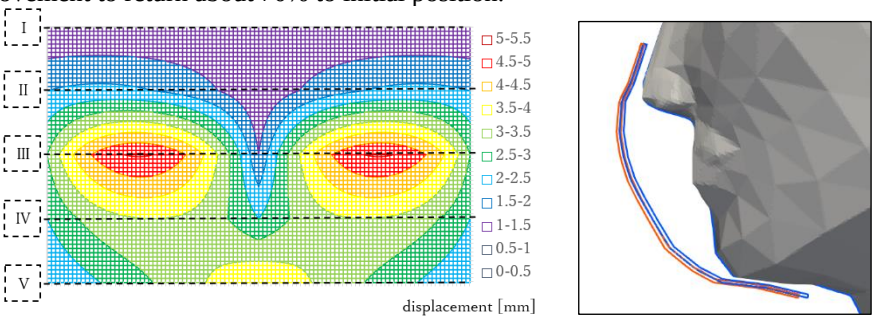

Fig.4. Visualization of maximum displacement (left) and a cross-sectional view of the mask (right): the blue line represents the original position, while the red line indicates the position of the mask at its maximum displacement.

ICCS Camera Ready Version 2024
To cite this paper please use the final published version:
DOI: 10.1007/978-3-031-63783-4_7

4 Simulation of Human Model Wearing Mask

4.1 Computational Mesh and Conditions

Figure 5 shows the computational domain for our simulations, with dimensions of 6.25 x 6.25 x 3.75 meters. To simplify the model and reduce computational complexity, the human body model excludes the lower body and both arms, standing 0.9 meters tall. The face mask model in the simulation is 2.5 mm thick to allow for the creation of at least three computational grids along its thickness. Initially, the gap between the face mask and the nose is set at 3.5 mm [19][20]. The coordinate system used is defined as follows: *x* represents the lateral direction relative to the human model, *y* is the vertical direction, and *z* is the direction facing forward from the human model.

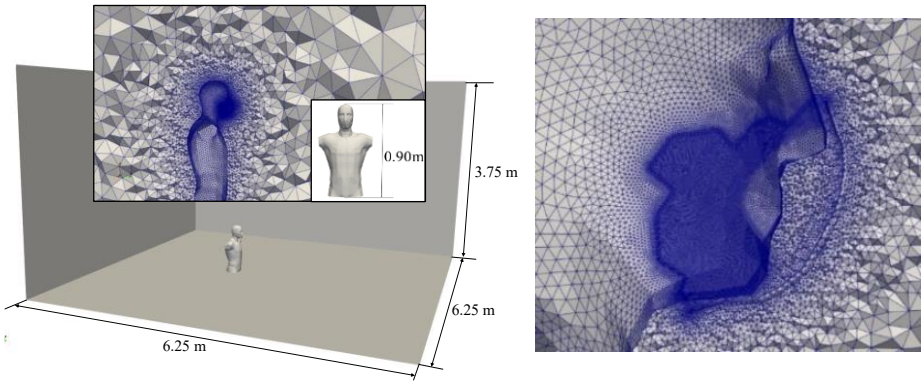

Fig.5. Overview of the computational domain and the grid surrounding the face mask

Computational grids were generated using MEGG3D software. The mesh distribution is detailed in the cross-sectional views of the computational grid at the center of the human body. The grids are more refined around the face mask. The total number of computational grids is approximately 2 million. The mouth of model is shaped as a rectangle, measuring 10 mm in height and 40 mm in width, with the smallest cell size being 0.5 mm.

Coughing begins at time $t = 0$ s and breathing begins after the coughing ends. To simulate the exhalation during coughing, we used volume flow rates recorded from a spirometer test [17]. The breathing volume flow rate was obtained from experimental measurements [21]. For the boundary condition of velocity at the mouth, the volume flow rate was divided by the mouth area of the model. We set the ceiling of the room as an outflow surface, the face mask and human body are no-slip walls. The motion of droplets was simulated at a temperature of 25℃ and a humidity of 60%. Initially, droplets were positioned in front of the mouth, with a total count of 10,000 droplets. To model realistic droplet behavior, we utilized the frequency distribution of droplet diameters expelled during coughing [22][23]. Droplets were considered adhered upon crossing any boundary. The motion of the droplets was calculated using pre-calculated unsteady flow velocity data, which was updated every 1/600 of a second.

ICCS Camera Ready Version 2024
To cite this paper please use the final published version:
DOI: 10.1007/978-3-031-63783-4_7

4.2 Result of Fluid Flow Simulation

Fig.6 shows the cross-sectional velocity distribution of the human body center at 0.1, 0.3 and 0.4 seconds. From the figure, it is observed that 0.1 seconds after the start of a cough, the mask moves forward, widening the airflow path between the mask and the human body. As a result, the flow velocity between the nose and the mask is reduced in the dynamic mask scenario.

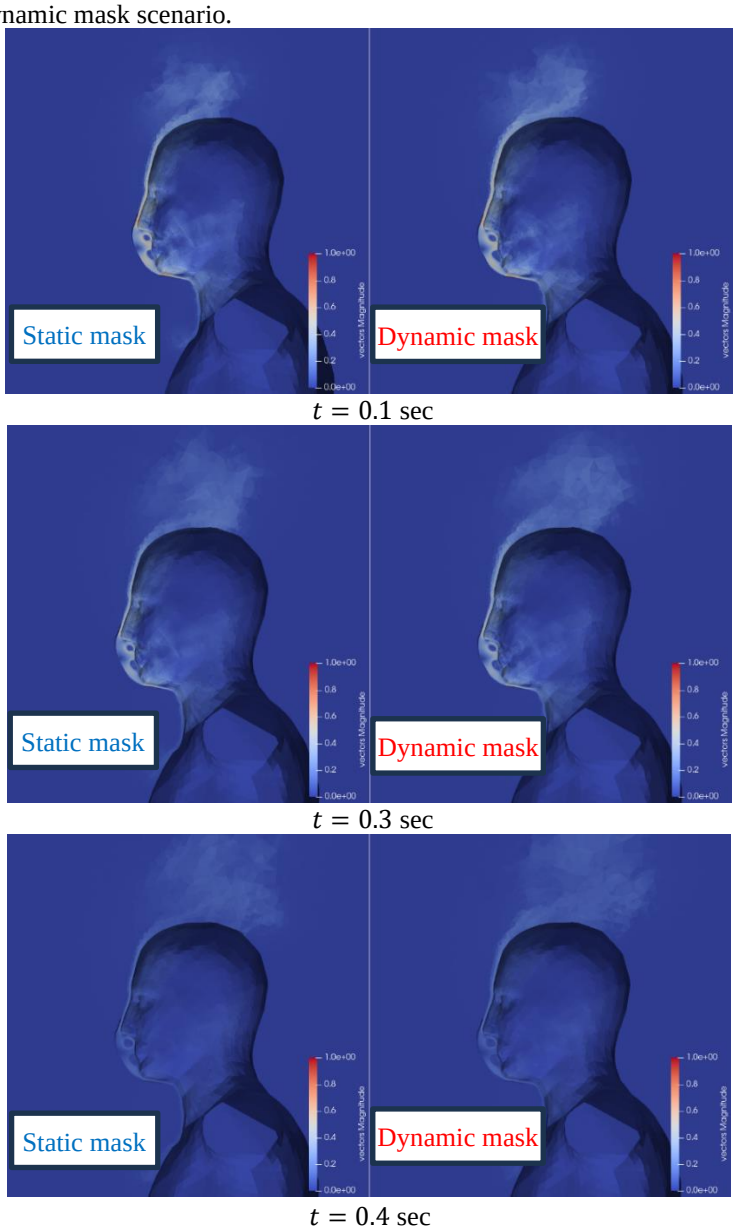

Fig.6. Comparison between static and dynamic mask with velocity distribution

ICCS Camera Ready Version 2024
To cite this paper please use the final published version:
DOI: 10.1007/978-3-031-63783-4_7

At 0.4 seconds, the flow tends to spread backward with the dynamic mask, while with the static mask, the tendency is for the flow to spread upward over the human body. Next, the average flow velocity in the gap between the mask and the human body model is shown in Fig. 7. The elements of the gap between the mask and the human body model used to calculate the average flow velocity are in the area shown in the inset of Fig. 7. The average flow velocity, at the time of maximum flow velocity, was about 7% lower with the dynamic mask compared to the static mask. This is due to the movement of the mask, which widened the flow path in the gap between the mask and the human body model. In the case of the static mask, the mask is on average about 3mm away from the human body model, while with the dynamic mask, the gap area between the mask and the body increased by up to about 6%.

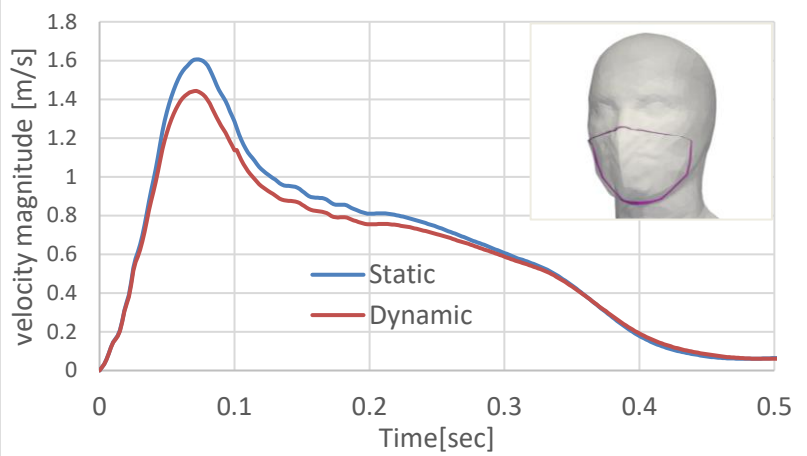

Fig.7. Average velocity magnitude of cells between mask and face during coughing

4.3 Result of Droplet Motion Simulation

Fig.8 (a) shows the positions of droplets at $t = 0.4, 4.0$ s, where red particle is the result using the flow velocity data of the Dynamic mask case and blue one is the result using the data of the Static mask case. The droplets adhering to the face mask and the human body are not drawn, and thus we can observe only the floating droplets shown at each time. In the Static mask case, the dispersion distance of droplets in the positive y direction was greater than Dynamic mask case. In addition, the average direct distance from the initial position of droplets was about 12% smaller with the Dynamic mask case than with the Static mask case, because of the flow velocity decreasing written in the last section. Consequently, the Dynamic mask was effective comparing to the Static mask to suppress the moving distance of droplets.

Next, we set some boxes around the human model as Bale et al. [4], and investigated the relationship between the number of droplets reaching each box and the total droplets volume, in 0.0-0.5 seconds. To identify where droplets leaked the most through the top of face mask, the side of face mask, and lower of face mask, boxes were sized to completely cover each gap illustrated in Fig.8. The size of the boxes was

ICCS Camera Ready Version 2024
To cite this paper please use the final published version:
DOI: 10.1007/978-3-031-63783-4_7

$140 \times 120 \times 20$ mm at the top, $160 \times 24 \times 44$ mm at the side, and $140 \times 320 \times 52$ mm at the bottom. Table 1 summarizes the number of droplets and the total volume of droplets that reached each box.

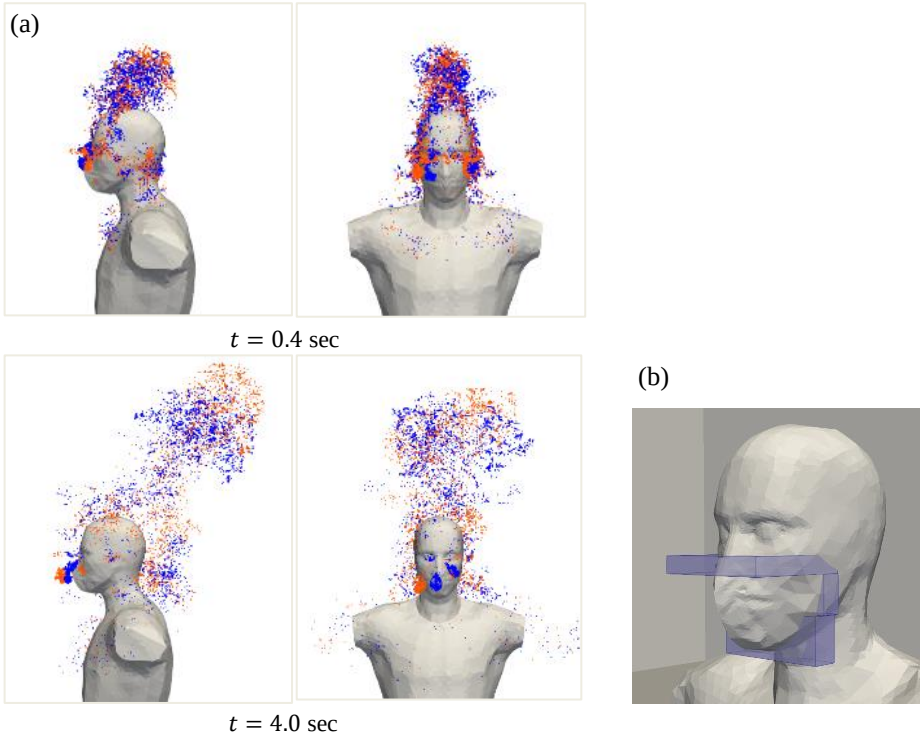

Fig.8. (a) Distribution of virus-laden droplets: Blue droplets result from using a static mask, while red droplets are from a dynamic mask and (b) position of boxes counting droplets.

Table 1. Number of droplets and volume in each box

	Number of droplet		Droplet volume [$\times 10^{-6}$ ml]	
	Static	Dynamic	Static	Dynamic
Top box	2997	2823	4.5	5.3
Side box(right)	216	226	5.2×10^{-2}	5.9×10^{-2}
Side box (left)	188	195	6.1×10^{-2}	5.7×10^{-2}
Lower box	334	323	6.3×10^{-2}	6.1×10^{-2}

We found that the number of leaked droplets were much larger on the top of the face mask compared to the sides and lower of the face mask. Next, we focus on the top parts, the number of droplets in the Dynamic mask case reduced by about 5.8% compared to the static mask case. However, the total volume of droplets increased by 18% in the dynamic mask. Large-diameter droplets tended to leak out from the top by considering the displacement of the mask. It is considered that this trend is because the wider gap

ICCS Camera Ready Version 2024
To cite this paper please use the final published version:
DOI: 10.1007/978-3-031-63783-4_7

caused large-diameter droplets, which has adhered to the Static mask, to flow out of the face mask without adhering to the face mask.

5 Applicational Computation

5.1 Transplant Calculation for Dynamic Mask

The above computation considering deforming a mask is high cost because very fine mesh is required around in/around the mask. To reduce computational costs, calculations within the mask are omitted. Instead, a model that fills the gap between the mask and the human body model, highlighted in red in Fig. 9 (left), is created. Inflow boundary condition is applied to this gap, using the flow velocity from the dynamic mask. Specifically, the flow velocity for the transplant calculation references the value from the cell whose element centroid is closest to the centroid of the boundary surface on the new gap. This approach is referred to as the transplant calculation in this study. Fig. 9 (right) compares the cross-sectional meshes for transplanted computation with those from a full computation in a dynamic mask, demonstrating that the area inside the mask, which previously occupied a significant portion of the computational grid, has been reduced. The new grid for the transplant calculation maintains the same number of elements (approximately 2 million) as that used in the dynamic mask calculation to facilitate a fair comparison of calculation times. The transplant calculations introduce a minor modification to the droplet calculations. The initial conditions for the droplets (coordinates, velocity, droplet diameter) in the transplant calculations are derived from their state at the moment they were ejected from the mask in the dynamic calculations. Consequently, the initial number of droplets for the transplant calculation was set at 3248, matching the count of droplets that emerged from the mask gaps in the dynamic mask droplet calculation.

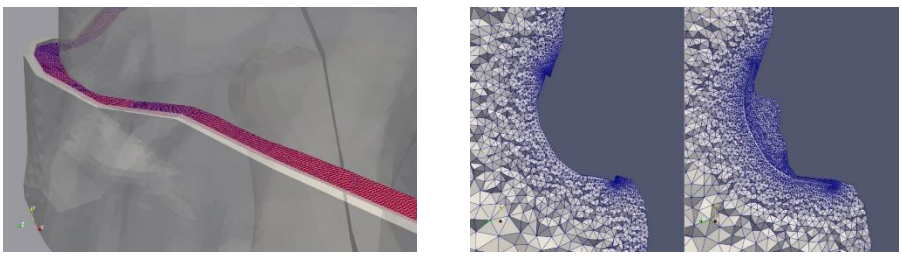

Fig.9. Gap-filled mask model（left), and a comparison of cross-sectional meshes for transplanted computation versus full computation in a dynamic mask (right)

The results of the transplant calculation, compared to those of the dynamic mask, are shown in Fig. 10. Fig. 10 (a) and (b) display the velocity distribution in a cross-section at the center of the human body at 0.1 seconds, representing the results of the dynamic and the transplant calculations, respectively. In the transplant calculation, since the inside of the mask is outside the computational domain, there is no data inside the mask. It can be seen that the tendency for the flow to spread backward is also reproduced in

ICCS Camera Ready Version 2024
To cite this paper please use the final published version:
DOI: 10.1007/978-3-031-63783-4_7

the transplant calculation. Moreover, by transplanting data from the dynamic mask, it is possible to replicate the reduction in flow velocity in the gap between the mask and the human body. The results of the droplet calculation using the airflow data from the transplant calculation are shown in Fig. 10 (c). The blue droplets represent the results of the transplant calculation, and the red droplets represent the results of the dynamic calculation. Although there are some differences in the motion of the droplets, it is evident that the transplant calculation can replicate the trend of droplets flowing backward, as seen in the dynamic mask calculation. The transplant calculation has reduced the computation time by approximately 56% compared to the calculation considering the movement of the mask.

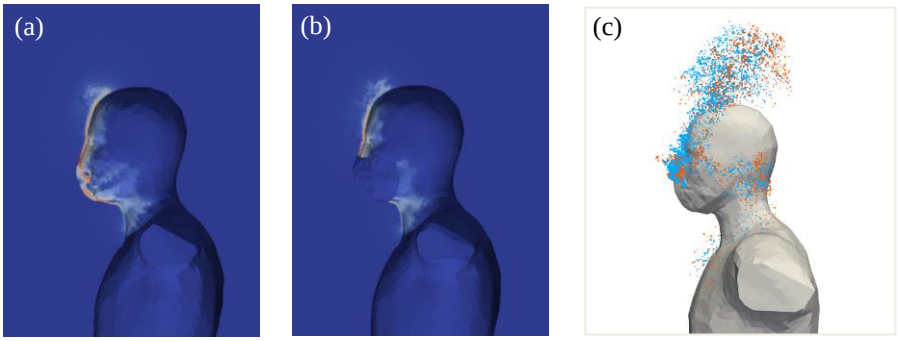

Fig.10. Distribution of flow velocity magnitude at 0.1 seconds in (a) the dynamic mask model and (b) the transplant model. (c) shows a comparison of droplet dispersion at 0.4 seconds.

5.2 Setting Up the Pushing Wheelchair Scenario

The transplant calculation significantly reduced computational costs while retaining the characteristics of the dynamic mask. From the calculations so far, it has been observed that droplets scatter further backward when using a dynamic mask on a human model compared to a model with a static mask. This indicates an increased risk of infection behind a mask-wearing individual. Therefore, as an applied calculation, we consider the scenario of pushing a wheelchair, where the infection probability increases behind the mask wearer. The computational model is shown in Fig. 10. It is assumed that the wheelchair does not significantly affect the movement of droplets scattered near the rear of the human body, and it is omitted to reduce the number of grids and simplify the model. The size of the whole computational domain is set to $8.0 \times 8.0 \times 6.0$ m. The grid width becomes finer around the mask and between the human models through which the droplets pass. The minimum grid width is about 0.5 mm. Transplant calculations using the airflow from the dynamic mask are applied to the human model wearing the mask. Furthermore, assuming a state of moving forward while pushing a wheelchair, a uniform flow is applied from the front. The propulsion speed of the wheelchair in straight-line motion is reported to be approximately 1 m/s, and it is noted that the sense of anxiety and fear of the occupant increases with speed [24]. Therefore, inflow speeds of 0.0, 0.5, 1.0, 1.5 m/s are set, and the number and volume of droplets passing around the respiratory area of the human model behind the infected person are

ICCS Camera Ready Version 2024
To cite this paper please use the final published version:
DOI: 10.1007/978-3-031-63783-4_7

investigated at each speed. Under the condition of providing inflow from the front, pre-calculations are performed until the flow develops to stabilize the flow caused by the uniform stream from the front, and then the cough velocity are transplanted. The boundary conditions are set as outflow for the ceiling, sides, and rear wall, with the mask and human body being no-slip wall.

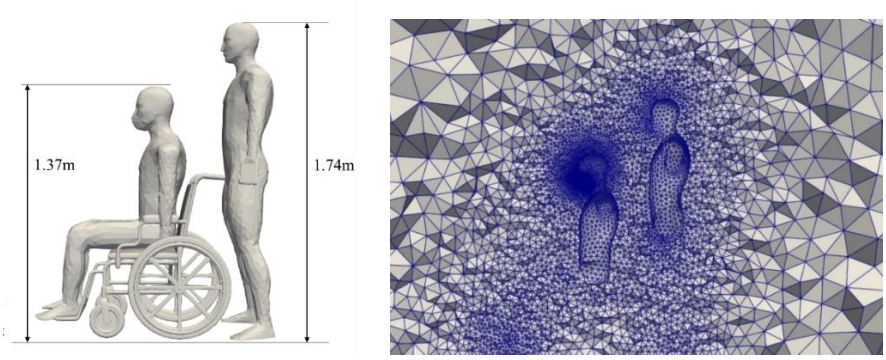

Fig.10. Model of a seated human wearing a face mask and a standing human (left), and computational mesh (right).

5.3 Results of the Pushing Wheelchair Scenario

To assess the risk of infection, a box is placed near the mouth of an infected individual, and the relationship between the number of droplets reaching the box and the total volume of droplets is investigated from 0.0 to 3.0 seconds after the start of a cough. The size of the box is determined based on the volume of air a typical adult inhale at once, set to 10×15×10 cm^3, following Bale et al. [2]. The number of droplets reaching the box and their total volume at each forward speed are shown in Fig. 11. Additionally, the state of droplets at 0.1, 0.55 and 1.0 seconds after the start of the cough is depicted in Fig. 12.

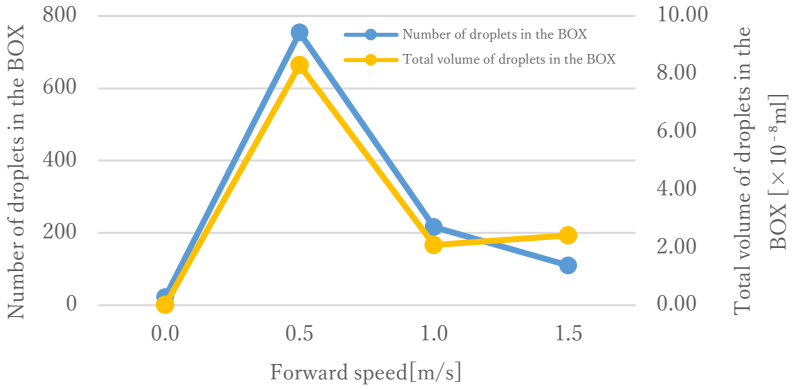

Fig.11. Number of droplets and total droplet volume in the BOX, counted at each wheelchair pushing speed

ICCS Camera Ready Version 2024
To cite this paper please use the final published version:
DOI: 10.1007/978-3-031-63783-4_7

When the wheelchair is stationary, droplets hardly reach the box placed near the respiratory area of the rear human model. When the wheelchair is pushed at a speed of 0.5 m/s, the highest number of droplets reach the box, and the total volume of droplets is also the largest. As the speed increases to 1.0 m/s and 1.5 m/s, the number of droplets reaching the box decreases, but the total volume of droplets reaching the box at 1.5 m/s is larger than at 1.0 m/s. This is believed to be because larger droplets are carried further backward due to the increased inflow from the front. Therefore, under the conditions of this study, the result shows that moving forward at a speed of about 0.5 m/s while pushing a wheelchair with an infected mask-wearer seated in it presents the highest risk of infection.

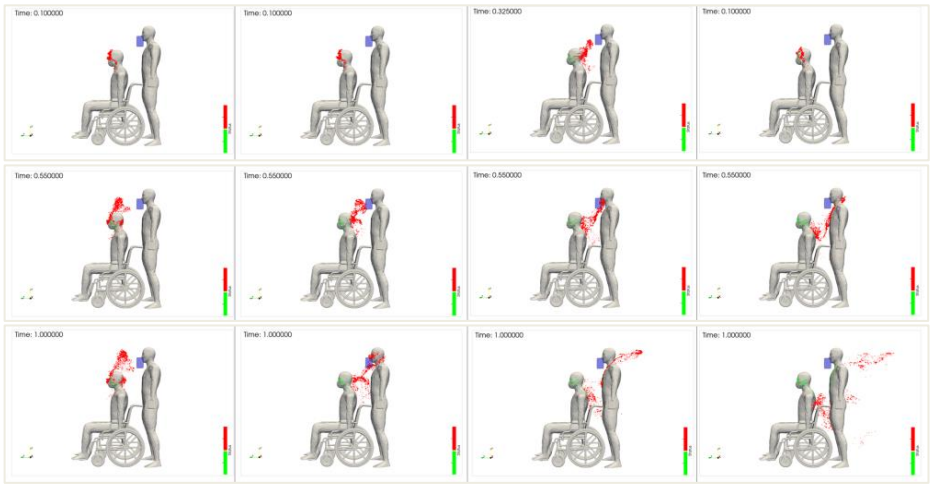

(a) 0.0 m/s (b) 0.5 m/s (c) 1.0 m/s (d) 1.5 m/s

Fig.12. Droplets dispertion at each forward speed at 0.1, 0.55 and 1.0 seconds after the start of the cough

6 Conclusion

To investigate the impact of face mask deformation caused by coughing on droplet behavior, we conducted a numerical simulation that integrated fluid flow and droplet motion. By measuring the displacement of the mask and applying dynamic fluid calculations that accounted for these displacements, we captured changes in droplet trajectories. Our findings revealed that coughing while wearing a disposable mask can result in approximately 6mm of mask displacement, accompanied by puffing out of the mask. In scenarios where the mask's dynamic behavior was considered, there was a 7% decrease in the average flow velocity in the gap between the mask and the human body, compared to using a static mask. Initially, droplets dispersed more rapidly when using a static mask; however, over time, the dynamic mask scenario allowed for a greater dispersion distance, with droplets spreading further backward. Additionally, we applied

ICCS Camera Ready Version 2024
To cite this paper please use the final published version:
DOI: 10.1007/978-3-031-63783-4_7

our findings to practical scenarios, such as assessing infection risk when pushing a wheelchair from behind. The simulation indicated that a caregiver pushing an infected individual who is wearing a mask at a speed of about 0.5 m/s faces the highest infection risk. It's important to note that these calculations were conducted assuming no obstructions at the head of the human model. This suggests that implementing barriers, such as wearing a hat, might obstruct airflow from the nose towards the head and potentially reduce the risk of infection.

Acknowledgements

This work was partially supported by JST CREST Grant Number JPMJCR20H7 and by JSPS KAKENHI Grant Number 21K03856.

References

1. World Health Organization, https://www.who.int/emergencies/diseases/novel-coronavirus-2019/question-and-answers-hub, last accessed 2024/2/29
2. Bale, R., Iida, A., Yamakawa, M., Li, C. and Tsubokura, M.: Quantifying the COVID19 infection risk due to droplet/aerosol inhalation. Scientific reports 12(1), 11186 (2022)
3. Yamakawa, M., Kitagawa, A., Ogura, K., Chung, Y.M. and Kim, M.: Computational investigation of prolonged airborne dispersion of novel coronavirus-laden droplets. Journal of aerosol science 155, 105769 (2021)
4. Bale, R., Li, C.G., Yamakawa, M., Iida, A., Kurose, R. and Tsubokura, M.: Simulation of droplet dispersion in COVID-19 type pandemics on Fugaku. In: Proceedings of the platform for advanced scientific computing conference, pp. 1-11. (2021)
5. Armand, P. and Tâche, J.: 3D modelling and simulation of the dispersion of droplets and drops carrying the SARS-CoV-2 virus in a railway transport coach. Scientific Reports 12(1), 4025 (2022)
6. Takii, A., Yamakawa, M., Kitagawa, A., Watamura, T., Chung, Y.M. and Kim, M.: Numerical model for cough-generated droplet dispersion on moving escalator with multiple passengers. Indoor air 32(11), e13131 (2022)
7. Dbouk, T. and Drikakis, D.: On coughing and airborne droplet transmission to humans. Physics of Fluids 32(5) (2020)
8. Bourouiba, L.: Turbulent gas clouds and respiratory pathogen emissions: potential implications for reducing transmission of COVID-19. Jama 323(18), 1837-1838 (2020)
9. Blocken, B., Malizia, F., van Druenen, T. and Marchal, T.: Towards aerodynamically equivalent COVID19 1.5 m social distancing for walking and running. preprint (1) (2020)
10. Bagchi, S., Basu, S., Chaudhuri, S. and Saha, A.: Penetration and secondary atomization of droplets impacted on wet facemasks. Physical Review Fluids 6(11), 110510 (2021)
11. Bourrianne, P., Xue, N., Nunes, J., Abkarian, M. and Stone, H.A.: Quantifying the effect of a mask on expiratory flows. Physical Review Fluids 6(11), 110511 (2021)
12. Pendar, M.R. and Páscoa, J.C.: Numerical modeling of the distribution of virus carrying saliva droplets during sneeze and cough. Physics of Fluids 32(8) (2020)
13. Dbouk, T. and Drikakis, D.: On respiratory droplets and face masks. Physics of Fluids 32(6) (2020)

ICCS Camera Ready Version 2024
To cite this paper please use the final published version:
DOI: 10.1007/978-3-031-63783-4_7

14. Takii, A., Yamakawa, M., Asao, S. and Tajiri, K.: Six degrees of freedom flight simulation of tilt-rotor aircraft with nacelle conversion. Journal of Computational Science 44, 101164 (2020)
15. Seokkwan Yoon.: Lower-Upper Symmetric-Gauss-Seidel Method for the Euler and Navier-Stokes Equations. In: AIAA Journal, Vol26No.9 (1988), pp.1025-1026.
16. Yamakawa, M., Kitagawa, A., Ogura, K., Chung, Y.M. and Kim, M.: Computational investigation of prolonged airborne dispersion of novel coronavirus-laden droplets. Journal of aerosol science 155, 105769 (2021)
17. Jitendra K. Gupta, Chao-Hsin Lin, and Qingyan Chen.: Flow Dynamics and Character-ization of a Cough. In: Indoor Air, 19, pp.517-525(2010)
18. Jitendra K. Gupta, Chao-Hsin Lin, and Qingyan Chen.: Characterizing Exhaled Airflow from Breathing and Talking. In: Indoor Air, 20, pp.31-39(2010)
19. Khosronejad, A., Santoni, C., Flora, K., Zhang, Z., Kang, S., Payabvash, S. and Sotiropoulos, F.: Fluid dynamics simulations show that facial masks can suppress the spread of COVID-19 in indoor environments. Aip Advances 10(12) (2020)
20. Talib Dbouk and Dimitris Drikakis.: On respiratory droplets and face masks. In: Phys-ics of Fluids 33,073315(2021)
21. Wallace O. Fenn, Hermann Rahn.: Handbook of physiology, Section3: Respiration, American Physiological Society Washington DC (1965).
22. J. P. Duguid et.: The size and the duration of air-carriage of respiratory droplets and droplet-nuclei. Epidemiology & Infection 44, 6, pp 471-479 (1946).
23. Shinhao Yang, Grace W M Lee, Cheng-Min Chen et.: The size and concentration of droplets generated by coughing in human subjects. In Journal of Aerosol Medicine, Vol.20 No.4, (2007), pp.484-494.
24. Noto, H., Saito, S., Muraki, S.: Influence of Wheelchair Pushing Speed on Riding Comfort and Helpers Physical Strain on Helpers. Japanese Journal of Nursing Art and Science 8(2), 37-45 (2009)

ICCS Camera Ready Version 2024
To cite this paper please use the final published version:
DOI: 10.1007/978-3-031-63783-4_7